Available online at www.sciencedirect.com

ScienceDirect

Energy Procedia 124 (2017) 834–841

Energy Procedia

www.elsevier.com/locate/procedia

7th International Conference on Silicon Photovoltaics, SiliconPV 2017

Enablers for IBC: integral cell and module development and implementation in PV industry

Ilkay Cesar[a], Nicolas Guillevin[a], Agnes A. Mewe[a], Pierpaolo Spinelli[a], Antonius R. Burgers[a], Victor Rosca[a], Lars A.G. Okel[a], Bart J. Geerligs[a], Arthur W. Weeber[a], Simon Sawallich[b], Michael Nagel[b]

[a]*Energy Research Center of the Netherlands, PO Box 1, 1755 ZG Petten, The Netherlands*
[b]*Protemics GmbH, Otto-Blumenthal-Str. 25, 52074 Aachen, Germany*

Abstract

An integral solar cell and module concept is developed based on an IBC cell design with a front floating emitter (FFE). The FFE renders the cell resilient to electrical shading and reduces the demands on feature size. The cells are bi-facial by design. We interconnected 6'' IBC cells using a conductive back sheet foil, resulting in a visually appealing mono-facial solar module. The IBC cells are made using a process close to existing industrial n-PERT processing, their production in an industrial pilot line has been demonstrated. The cells can be produced at the cost level of a PERC cell. The paper shows how the current cell efficiency of 21.1% cell will be increased beyond 22% in 2017 and what enablers are required to industrialize this concept. One such enabler we report on is high resolution R_{sheet} mapping using near-field THz scanning.

Peer review by the scientific conference committee of SiliconPV 2017 under responsibility of PSE AG.

Keywords: back contact; solar cell; silicon; module; near field; TeraHz

1. ECN's Front Floating Emitter (FFE) IBC cells

The Mercury cell [1,2] is ECN's 6 inch industrial Interdigitated Back Contact (IBC) cell design with a front floating emitter (FFE). A cross-section of the cell is shown in Fig. 1. Although interdigitated back contact (IBC) solar cells have shown to yield very high conversion efficiencies [3], cost effective production of these devices poses challenges. To allow all contacts to be applied to the rear of the cell, the rear collecting junction (the emitter) is interrupted by a non-collecting junction (the BSF) as again illustrated in Fig. 2. Therefore, any carrier that is photo-generated above a BSF area needs to travel laterally to an emitter area. If the BSF regions become too wide, the

1876-6102
Peer review by the scientific conference committee of SiliconPV 2017 under responsibility of PSE AG.
10.1016/j.egypro.2017.09.355

collection probability of carriers generated above the BSF will decrease: an effect referred to as electrical shading [4].

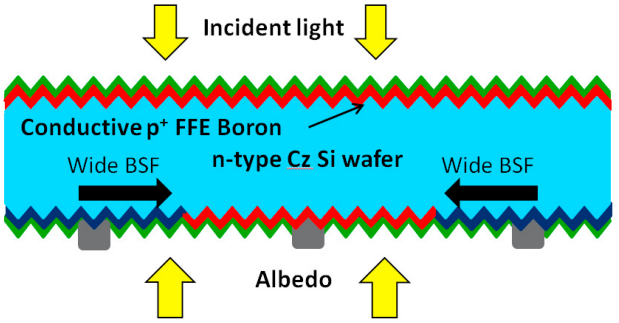

Fig. 1. cross-section of Front Floating Emitter Mercury cell. The rear side can receive light, except for where the metallization is present.

To prevent loss in cell performance, the typical width of the BSF is in the order of 0.2-0.4 mm out of a typical cell pitch of 1.5 mm. The inequality of BSF and emitter widths results in strict patterning tolerances for processing but has also implications for the metallization as shown in our previous report [1]. We found that an FFE can mitigate this effect. To illustrate why the IBC structure with FFE can allow wide features on the cell, we compare 2D Quokka [5] simulations of an interdigitated structure featuring extreme widths with FSF or FFE on the front side in Fig. 2.

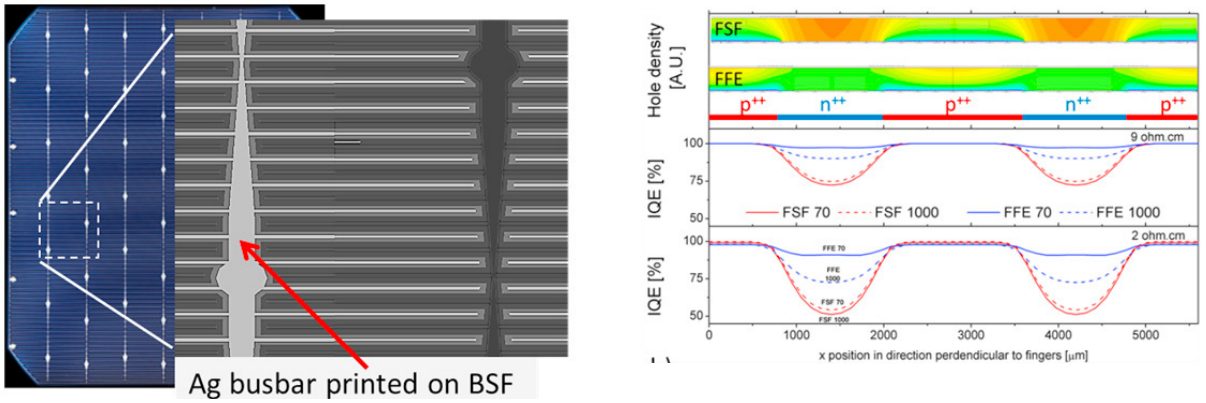

Fig. 2. (left) relatively wide pattern features to allow current extraction; (right) reduced electrical shading for conductive FFE vs. FSF for extremely wide BSF (1.2 mm).

From the hole density plots it is clear that the hole distribution and the local current collection probability (IQE) is radically different between both structures. While the IQE above the n++ doped region (BSF) drops 25 to 50% for the case with FSF depending on the wafer resistance, the IQE of the FFE-IBC remains nearly constant over the interdigitated structure, depending on the conductance of the FFE. While a conductive FFE is beneficial to counter electrical shading, reasonable results are expected to be achieved between 100 and 200 Ω/□ which is a range in which very good surface passivation can be achieved. While we have obtained 36 fA/cm^2 at 150 Ω/□, even lower values of 10 fA/cm^2 were obtained by others at 185 Ω/□ on textured surfaces.

Another important consequence of the Mercury concept is that it allows the doping pattern to deviate from the regular interdigitated structure. With the regular interdigitated structure we mean the pattern with horizontally running fingers that can be observed in Fig. 2. Here the interdigitated doping pattern is interrupted by a mini busbar which has a tapered structure towards the interconnection pad. Deviations in this interdigitated structure (busbars

and pads) are required to be able to extract the current from the cell. The FFE allows to use these current extraction features, without a large penalty in the form of electrical shading. This is very beneficial in order to establish cost effective interconnection on 6 inch wafers. To limit ohmic losses and/or metal consumption on the cell, it is beneficial to collect the current close to the location where the photocurrent is generated in the solar cell.

Others have reported on IBC solar cells, e.g. Müller et al [6] reported an attractive process flow for an FFE IBC cell that reached 21.7% on 2x2 cm^2 based on P-implantation that selectively blocked the following BBr_3 diffusion. The screen printed 6 inch IBC cells that ISC Konstanz [7] has reported achieved 22.0% efficiency. These cells also feature a FFE illustrating the potential of this low-cost approach.

2. Cell and module process

The processing of our IBC cells is based upon our n-pasha process for n-PERT cells [8]. A big advantage of this approach is that the process is suitable for transfer to industry. Tube diffusion, screen printing and use of firing through metallization are important characteristics of this technology.

Our cells are currently designed to be interconnected with conductive back sheets [9-11], technology that was developed originally for back contact MWT cells. The back contact module based on the conductive back-sheet technology has a track record of being a reliable interconnection, meeting IEC 61215 demands, and using commercial pick & place module manufacturing tools. The interconnection between the cell metallization and the back contact foil is achieved through conductive adhesive. This interconnection technology by itself has potential for improvement and further cost reduction, as reported in [12].

The IBC cells that are free of front metallisation give the module an aesthetical appearance as illustrated in Fig. 3. Recently, ECN has fabricated its first 60 cell IBC module illustrating the manufacturability of the technology.

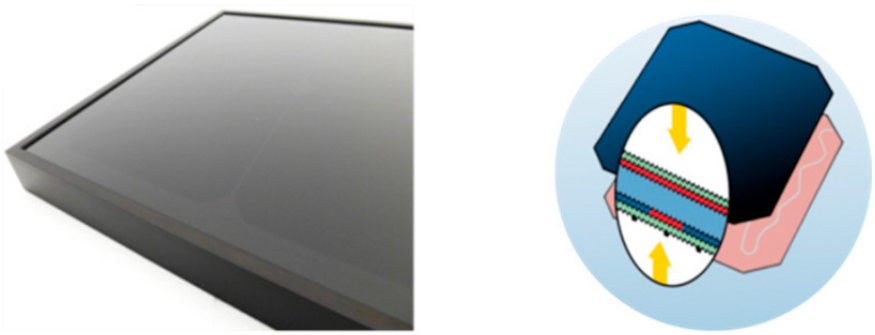

Fig. 3. (left) Photographic image of an all-black 2x2 IBC module; (right) Illustration of an IBC cell on conductive back-sheet foil. The IBC cell (dark blue) is mounted on a patterned conductive back-sheet (pink). The back-sheet has isolation trenches (light grey), separating the + and – polarities. In the circle a cross-section of the IBC cell is shown with the contacts to the n-type diffusion (blue) and the p-type diffusion (red) at the rear side.

3. Demonstration of IBC Mercury cells in an industrial pilot line

At Yingli [13] the IBC process has been transferred to an industrial pilot line in a time span of only 3 months. The I-V parameters of the best cell to date are listed in Table 1. The speedy transfer testifies to the potential for industrial application of the IBC Mercury cell.

Table 1: I-V parameters of best 6'' Mercury IBC cell processed at Yingli to date.

V_{oc} (mV)	J_{sc} (mA/cm^2)	FF (%)	Efficiency (%)
657	40.34	77.4	20.51

4. FFE-IBC efficiency evolution and bottlenecks

Early 2014 [1], we reported a first efficiency for the FFE-IBC concept on 6'' cells of up to 19.0%. We have been able to steadily increase the efficiency of our cells, and reported our best efficiency to date of 21.1%. The I-V parameters of this cell are listed in Table 2, based on in-house measurements.

Table 2: I-V parameters of the best FFE IBC cell and simulated efficiency potential.

	Area	J_{sc} (mA/cm^2)	V_{oc} (mV)	*FF* (%)	Efficiency (%)
Experimental	239	41.2	653	78.4	21.1
Simulation	239	41.2	658	80.9	22.0
delta		0	-0.8%	-2.9%	-3.7%

As mentioned earlier, a key characteristic of the current cell processing is firing through (FT) metallization. The challenge of FT metallization is to limit the contact recombination as the frit fraction in the paste etches into the diffusion during firing for a significant distance (about 200 nm estimated). This etching reduces the surface shielding effect of the diffusion, resulting in increased J_0 values but at the same time is also important to optimize contact resistance. In order to control and optimize the firing through process as much as possible, it is important to be able to characterize the metallization, for instance by measuring J_0 and contact resistance values of the metallization.

As shown in Table 2, the efficiency of our cells is lower than expected from device simulations. The difference is under investigation and factors like contact resistance and inhomogeneity of diffusions are likely to cause the difference. We investigate the homogeneity of the diffusions using near-field THz scanning, that is discussed in a later section. From the data presented here we can conclude that the potential for screen printed FT cells is 22%, and that there is room for improvement in our current cells, in particular in FF. By improving the contact properties that enable smaller contact areas, there is potential for further improvement beyond 22%, and work to demonstrate that is underway. See for instance [14].

To assess critical parameters, such as J_0 and r_c of the contacts, we designed special test patterns, to be measured with a custom measurement chuck, allowing to pin-point values of all these parameters [15]. Based on these measured J_0 values of contacts and passivated surfaces (see Table 3) as well as grid resistances we used device simulations to assess the efficiency for this solar cell configuration as tabulated in Table 2.

Table 3: J_0 values and contact coverage for the different scenarios.

		BSF	Emitter
J_0 (passivated)	fA/cm^2	230	57
J_0 (contacted)	fA/cm^2	1200	2000
metal coverage	%	7.6	4

5. Mapping of diffusion patterns with THz mapping

In the Mercury IBC cell the FFE has an important role in the lateral transport of holes. To assess the effectiveness of the pumping effect across the cell, it is also desirable to map the FFE sheet resistance. Also it is important to be able to control and monitor the patterning of the rear side. Typically, for BSF and emitter diffusions on the rear side one will target different sheet resistances. The differences in sheet resistance allow to monitor the accuracy of the patterning process. The doping profile near the surface is important for the contacting of the metallisation. In general, areas with a high sheet resistance will be more difficult to contact, and detailed maps will reveal areas that are more prone to high contact resistance, or spiking through the diffusion during firing.

Fortunately there is a way to map the sheet resistance with high resolution using THz near-field probing. In Fig. 4 the measurement principle is illustrated. The attenuation of the THz radiation is directly linked to the conductivity of

the diffusions. See [15,16] for a more detailed description of the high resolution R_{sheet} mapping. The method allows fast (5 ms/pixel) and contact less R_{sheet} mapping in a range of 0.5 Ω to 5 kΩ. Qualitative differences in R_{sheet} can be observed for features as small as 20 µm for ideal conditions.

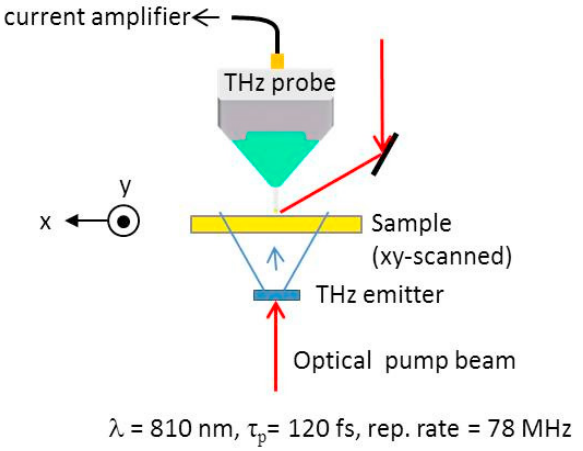

Fig. 4: Principle of the THz measurement

In Fig. 5 a sample scan is shown. The scan is of a test structure that has a homogeneous p^+-type diffusion on the front, but is patterned on the rear side. The rear pattern has larger squares of either emitter or BSF doping only on the rear, in the centre and the corners, used for instance for QSSPC lifetime measurements. At the edges there are 2 sections with interdigitated diffusion patterns, having a pitch of roughly 1 mm.

While in section a) the diffused fingers show a homogenous sheet resistances over the full length of the finger, elevated sheet resistances are observed towards one end of the fingers in section b) with R_{sheet} values of the emitter well above 100 Ω/□ (in red). This range in R_{sheet} can negatively affect both the resistive as well as recombination properties of the contacts and give clues towards performance losses and process improvements.

The THz equipment for PV is a co-development between Protemics and ECN. A full wafer mapping tool is available at ECN which will provide better feedback on our IBC process and that used in the PV community, and result in process improvements and efficiency gains.

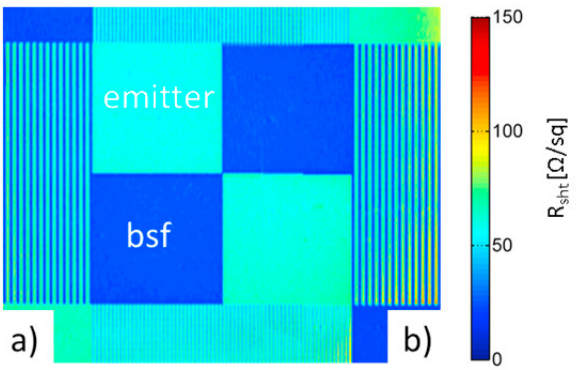

Fig. 5: THz mapping of IBC test structure (R_{sheet} in Ω/sq) illustrating interdigitated emitter fingers with (a) homogeneous Rsheet and (b) partly elevated R_{sheet}.

6. Market developments for back contact solar cells

The general trend in the market is to move to higher module power and a lower cost per watt-peak. In Fig. 6 several market developments as projected by the ITRPV [17] are shown. While p-type material with standard front and rear contact technology has dominated over the last decades, the ITRPV roadmap predicts an increasing share of back contact module technology and n-type material. A relatively new trend is the appearance of bifacial modules in the market.

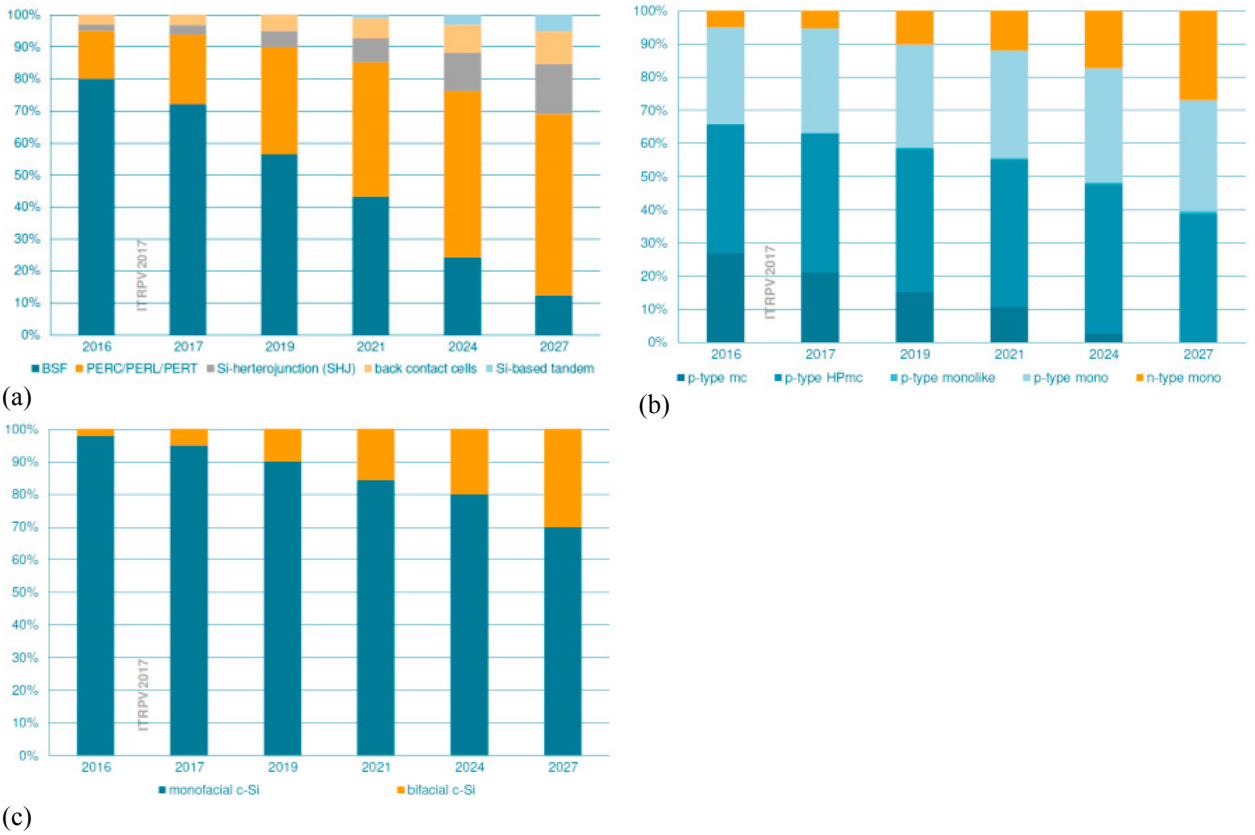

Fig. 6: possible market developments from the ITRPV roadmap, for (a) cell technology; (b) wafer type; (c) monofacial vs. bifacial technology. The vertical axes show the world market share.

We note that the Mercury IBC cells is a very good match to these developments, being a bifacial, back-contact and n-type solar cell.

7. Status Cost of ownership versus PERC

The development has resulted in a process flow for an IBC cell that has only one additional major process step compared to the commercial n-PERT cell with a homogeneous BSF. This and the fact that the patterning of the doped surface is based on screen printing, has attracted interest from PV manufacturers. In addition, further process simplification is feasible. This achievement places the process complexity next to that of PERC and marks a turning point with respect to the market perception that an IBC process is laborious and expensive. We were able to raise the IBC cell efficiency on 6 inch wafers from 19.5% in 2014 to 21.1% currently, using equipment of the consortium partners and an advanced metallization design based on screen printing. The process cost, excluding the cost for

wafer and silver paste, reached a cost level as low as 36.5 $ct/cell which is a cost level comparable to that of PERC. The cost breakdown in wafer, silver and process cost per watt-peak is illustrated in Fig. 7.

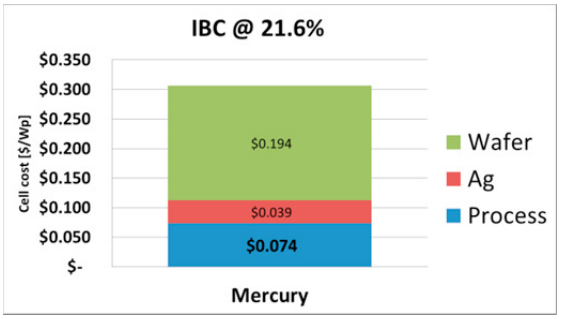

Fig. 7: Cell cost of current IBC process. The $/Wp is calculated assuming a 21.6% conversion efficiency

8. Conclusions

We present a bifacial IBC cell concept with a process close to current industrial processing, as highlighted by the quick transfer to an industrial pilot line. The best efficiencies reached to date are 21.1% at ECN, 20.5% in pilot at Yingli. These efficiencies must be improved to attain a viable business case, and will be improved, and for that it is important to be able to monitor and control the processing and cell parameters. Two examples of that shown in the paper are the use of test structures for J_0 and r_c values, and THz mapping for resolving interdigitated diffusion patterns.

References

[1] Cesar I, Guillevin N, Burgers AR, Mewe AA, Koppes M, Anker J, Geerligs LJ, Weeber AW. Mercury: A back junction back contact front floating emitter cell with novel design for high efficiency and simplified processing. Energy Procedia 2014; 55:633-42.
[2] Cesar I, Guillevin N, Burgers AR, Mewe AA, Bende EE, Rosca V, Van Aken BB, Koppes M, Anker J, Geerligs LJ, Weeber AW. Mercury: a novel design for a back junction back contact cell with front floating emitter for high efficiency and simplified processing. In 29th European Photovoltaic Solar Energy Conference, Amsterdam, The Netherlands, 2014.
[3] Xu G, Yang Y, Zhang X, Chen S, Liu W, Chen Y, Li Z, Chen Y, Altermatt PP, Verlinden PJ, Feng Z. 6 inch IBC cells with efficiency of 23.5% fabricated with low-cost industrial technologies. In 43rd IEEE Photovoltaic Specialists Conference (PVSC), p. 3356-59, 2016.
[4] Hermle M, Granek F, Schultz-Wittmann O, Glunz SW. Shading effects in back-junction back-contacted silicon solar cells. In 33rd IEEE Photovoltaic Specialists Conference, p. 1-4, 2008.
[5] Fell A. A free and fast 3D/2D solar cell simulator featuring conductive boundary and quasi-neutrality approximations. IEEE Trans. on Electron Devices 2012; 60(2):733-8.
[6] Mueller R, Schrof J, Reichel C, Benick J, Hermle M. Back-junction back-contact n-type silicon solar cell with u diffused boron emitter locally blocked by implanted phosphorus. Appl. Phys. Lett. 2014;105:103503.
[7] Halm A, Mihailetchi VD, Galbiati G, Koduvelikulathu LJ, Roescu R, Comparotto C, Kopecek R, Peter K, Libal J. The zebra cell concept-large area n-type interdigitated back contact solar cells and one-cell modules fabricated using standard industrial processing equipment. In 27th European Photovoltaic Solar Energy Conference, Frankfurt, Germany, 2012.
[8] Romijn IG, Anker J, Burgers AR, Gutjahr A, Heurtault B, Koppes M, Kossen E, Lamers MWPE, Saynova DS, Tool CJJ. Industrial cost effective n-pasha solar cells with > 20% efficiency. In 28th European Photovoltaic Solar Energy Conference, Paris, France, 2013.
[9] Lamers MWPE, Tjengdrawira C, Koppes M, Bennett IJ, Bende EE, Visser TP, Kossen EJ, Brockholz B, Mewe AA, Romijn IG, Sauar E, Carnel L, Julsrud S, Naas T, De Jong PC, Weeber AW. 17.9% Metal-Wrap-Through mc-si cells resulting in module efficiency of 17.0%. In 25th Eurepean Photovoltaic Solar Energy Conference, Valencia, Spain, p. 1417, 2010
[10] Bennett IJ, Eerenstein W, Rosca V. Reducing the cost of back-contact module technology. Energy Procedia 2013; 38:329-33.
[11] Bende EE, Van Aken BB. The effect of reduced silver paste consumption on the cost per wp for tab-based modules and conductive-foil based modules. Energy Procedia 2015;67:163-74.
[12] Goris MJAA, Kikkert BWJ, Kroon JM, Rozema K, Bennett IJ, Verlaak J. Production of low cost back contact based PV modules. In 32nd European Photovoltaic Solar Energy Conference, Munich, Germany, p. 99-104, 2016.
[13] Z. Wang. IBC cell process for mass-production based on PANDA cell technology. In n-PV workshop 2017, Freiburg. To be published.
[14] Mewe AA, Spinelli P, Burgers AR, Vlooswijk AHG, Guillevin N, Kossen EJ, Cesar I. Emitter and contact optimization for high-efficiency IBC Mercury cells. In 32nd European Photovoltaic Solar Energy Conference, Munich, Germany, 2016.

[15] Spinelli P, Danzl P, Guillevin N, Mewe AA, Sawallich S, Vlooswijk AHG, Van de Loo BWH, Kessels WMM, Nagel M, Cesar I. High resolution sheet resistance mapping to unveil edge effects in industrial IBC solar cells. Energy Procedia 2016; 92:218-24.
[16] Nagel M, Safiei A, Sawallich S, Matheisen C, Pletzer TM, Mewe AA, Van der Borg NCJM, Cesar I, Kurz H. THz microprobe system for contact-free high-resolution sheet resistance imaging. In 29th European Photovoltaic Solar Energy Conference, Paris, France, pages 856-860, 2013.
[17] International technology roadmap for photovoltaic (ITRPV), 8th edition, 2017. http://www.itrpv.net/